arXiv:1901.06658v8 [physics.geo-ph] 16 Nov 2023

Geoelectric field and seismicity changes preceding the 2018 M_w6.8 earthquake and the subsequent activity in Greece

N. V. Sarlis,[1] E. S. Skordas,[1] and P. A. Varotsos[1,*]

[1] *Solid State Section and Solid Earth Physics Institute, Physics Department, University of Athens, Panepistimiopolis, Zografos 157 84, Athens, Greece*

A strong earthquake of magnitude M_w6.8 struck Western Greece on 25 October 2018 with epicenter at 37.515^{o}N 20.564^{o}E. It was preceded by an anomalous geolectric signal that was recorded on 2 October 2018 at a measuring station 70km away from the epicenter. Upon analyzing this signal in natural time, we find that it conforms to the conditions suggested (e.g., Entropy **2017**, 19, 177) for its identification as precursory Seismic Electric Signal (SES) activity. Notably, the observed lead time of 23 days lies within the range of values that has been very recently identified (Entropy **2018**, 20, 561) as being statistically significant for the precursory variations of the electric field of the Earth. Moreover, the analysis in natural time of the seismicity subsequent to the SES activity in the area candidate to suffer this strong earthquake reveals that the criticality conditions were obeyed early in the morning of 18 October 2018, i.e., almost a week before the strong earthquake occurrence, in agreement with earlier findings. Furthermore, upon employing the recent method of nowcasting earthquakes, which is based on natural time, we find an earthquake potential score around 80% just before the occurrence of this M_w6.8 earthquake. Here, we also report the recording of more recent SES activities including a very recent one which just appeared at Pirgos measuring station on 13 October 2023.

PACS numbers: 05.40.-a, 05.45.Tp, 91.30.Dk, 89.75.-k

I. INTRODUCTION

According to the United States Geological Survey (USGS) [1], a strong earthquake (EQ) of moment magnitude M_w6.8 occurred on 25 October 2018 22:55 UTC at an epicentral distance around 133 km SW of the city of Patras, Western Greece. Patras has a metropolitan area inhabited by a quarter of a million persons and fatal casualties have been probably avoided because, among others, at 22:23 UTC almost half an hour before the strong EQ a moderate EQ of magnitude M=5.0 occurred approximately at the same area as the strong EQ[2] (see Fig.1).

Geoelectric field continuous monitoring is operating in Greece by the Solid Earth Physics Institute[4–6] at 9 measuring field stations (see the blue circles in Fig.1) aiming at detecting Seismic Electric Signals (SES). SES are low frequency ($\leq$ 1Hz) variations of the electric field of the Earth that have been found to precede strong EQs in Greece[7–11], Japan[12–14], China[15–18], Mexico[19, 20], and elsewhere[21]. They are emitted due to the cooperative orientation of the electric dipoles [5, 22, 23] (that any how exist due to defects[24, 25] in the rocks) of the future focal area when the gradually increasing stress before the strong EQ reaches a critical value[10]. SES may appear either as single pulses or in the form of SES activities, i.e, many pulses within a relatively short time period ([9], e.g. see Fig.2). The lead time of single SES is less than or equal to 11 days while for SES activities it varies from a few weeks up to $5\frac{1}{2}$ months [6, 9]. SES are recorded[9, 10] at sensitive points[26] on the Earth's surface which have been selected after long experimentation in Greece during 1980s and 1990s that led[27, 28] to the construction of the so-called VAN telemetric network (from the acronym of the scientists Varotsos, Alexopoulos and Nomicos who pioneered this research) comprising the 9 measuring field stations depicted in Fig.1. Each measuring station records SES from specific EQ prone areas which constitute the so-called selectivity map of the station [3, 10, 29]. The gray shaded area of Fig.1 depicts the selectivity map for the Pirgos (PIR) measuring station as it resulted after the recording of SES from various epicentral areas [30]. A basic criterion for distinguishing SES from noise is that the recorded signal should[9] exhibit properties compatible with the fact that it was emitted far away from the recording station. This is usually called[9] $\Delta V/L$ criterion (where ΔV stands for the potential difference between two electrodes that constitute a measuring electric dipole and L for the distance between them) and has been found[31–34] to be compatible with the aforementioned SES generation model if we take into account that EQs occur in faults (where resistivity is usually orders of magnitude smaller than that of the surrounding rocks, e.g., see [5] and references therein).

The SES research has been greatly advanced after the introduction of the concept of natural time in 2001 [35–37]. Firstly, the criticality properties of SES activities (like the existence of long-range correlations and unique entropic properties) has been revealed by natural time analysis and hence new possibilities have been provided for the identification of SES and their distinction from man-made noise [11, 38–43]. Secondly, natural time analysis allowed the introduction of an order parameter for

*Electronic address: pvaro@otenet.gr

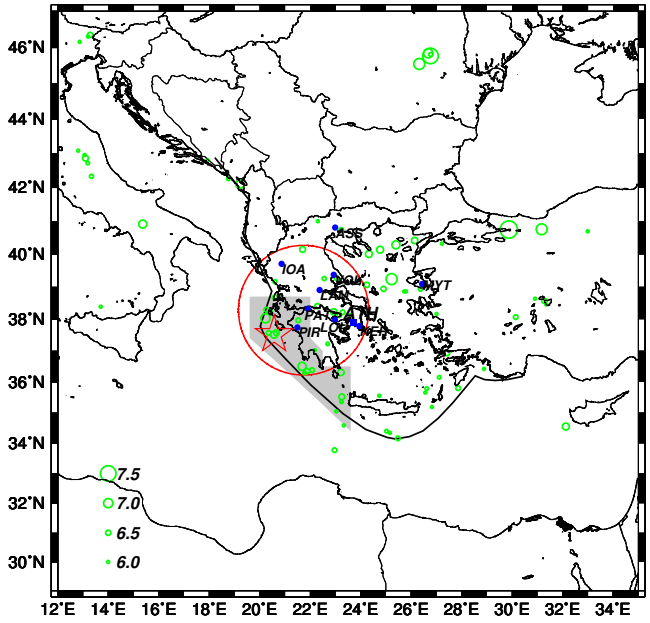


FIG. 1: (color online) Map of the larger area $N_{29}^{47}E_{12}^{35}$ in which the EQs of magnitude greater than or equal to 6.0 are shown by the green circles. The locations of the measuring stations operating in Greece of the VAN telemetric network are shown by the blue circles. The thick black line depicts the Hellenic arc[3] while the gray shaded area the selectivity map of Pirgos (PIR) measuring station. The red star corresponds to the epicenter of the M_w6.8 EQ on 25 October 2018 and the red circle delimits a circular region with radius $R = 225$km around the city of Patras.

seismicity the study of which allows the determination of the occurrence time of the strong EQ within a few days up to one week [6, 30, 40, 44–47]. Thirdly, minima of the fluctuations of the order parameter of seismicity have been identified before all shallow EQs with M $\geq$ 7.6 in Japan during the 27 year period from 1 January 1984 to 11 March 2011, the date of the M9.0 Tohoku EQ occurrence [48, 49]. Finally, the interrelation of SES activities and seismicity has been further clarified because when studying the EQ magnitude time series in Japan it was found that the minimum of the fluctuations of the order parameter of seismicity, which is observed simultaneously with the initiation of an SES activity [50], appears when long range correlations prevail [51].

The scope of the major part of this paper that appeared on 16 November 2018 in Ref.[52] by the first two authors was twofold: First, to report the geoelectrical field changes (SES) observed before the M_w6.8 EQ that occurred on 25 October 2018. Second, to present the natural time analysis of both the SES activity and the seismicity preceding this EQ. In this version, we present what happened after this M_w6.8 EQ including the additional SES activities recorded (Section IV) and updating the nowcasting results in subsection III.D a summary of our results and the main conclusions are presented in the final Section.

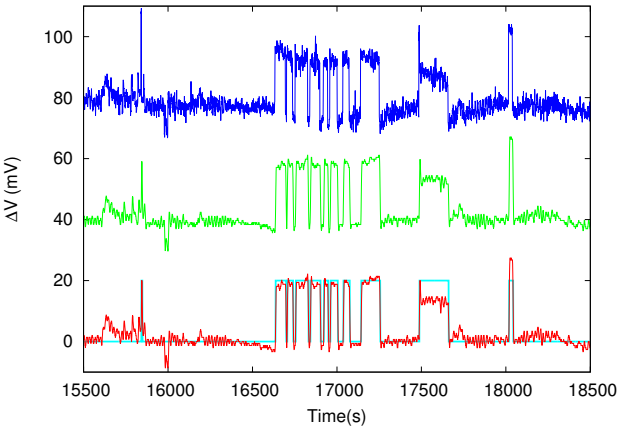


FIG. 2: (color online) The SES activity recorded at three (almost parallel) measuring dipoles at PIR station. The time is measured in seconds since 00:00 UTC on 2 October 2018. The dichotomous representation of the SES activity is shown in the bottom channel by the cyan line.

II. NATURAL TIME ANALYSIS. BACKGROUND

Natural time analysis, introduced in the beginning of 2000's [35–39], uncovers unique dynamic features hidden behind the time series of complex systems. In a time series comprising N events, the natural time $\chi_k = k/N$ serves as an index for the occurrence of the k-th event. This index together with the energy Q_k released during the k-th event, i.e., the pair (χ_k, Q_k), is studied in natural time analysis. Alternatively, one studies the pair (χ_k, p_k), where

$$p_k = \frac{Q_k}{\sum_{n=1}^{N} Q_n} \tag{1}$$

stands for the normalized energy released during the k-th event. As it is obvious from Eq.(1), the correct estimation of p_k simply demands that Q_k should be proportional to the energy emitted during the k-th event. Thus, for SES activities Q_k is proportional to the duration of the k-th pulse while for EQs it is proportional to the energy emitted[53] during the k-th EQ of magnitude M_k, i.e., $Q_k \propto 10^{1.5M_k}$ (see also [6, 54]). The variance of χ weighted for p_k, labeled by κ_1, is given by [6, 35, 38–40]

$$\kappa_1 = \sum_{k=1}^{N} p_k(\chi_k)^2 - \left(\sum_{k=1}^{N} p_k\chi_k\right)^2. \tag{2}$$

For the case of seismicity, the quantity κ_1 has been proposed to be an order parameter since κ_1 changes abruptly when a mainshock (the new phase) occurs, and in addition the statistical properties of its fluctuations are similar to those in other non-equilibrium and equilibrium

critical systems ([40], see also pp. 249-253 of Ref. [6]) . It has been also found that κ_1 is a key parameter that enables recognition of the complex dynamical system under study entering the critical stage [6, 35–37]. This occurs when κ_1 becomes equal to 0.070 ([55], see also p. 343 of Ref.[6]). In Table 8.1 of Ref.[6] one can find a compilation of 14 cases including a variety of dynamical models in which the condition κ_1=0.070 has been ascertained (cf. this has been also later confirmed in the analyses of very recent experimental results in Japan by Hayakawa and coworkers [56–58]). Especially for the case of SES activities, it has been found that when they are analyzed in natural time we find κ_1 values close to 0.070 ([35, 36, 38, 39], e.g. see Table 4.6 on p. 227 of Ref. [6]), i.e.,

$$\kappa_1 \approx 0.070. \quad (3)$$

When analyzing in natural time the small EQs with magnitudes greater than or equal to a threshold magnitude M_{thres} that occur after the initiation of an SES activity within the selectivity map of the measuring station that recorded the SES activity, the condition $\kappa_1 = 0.070$ is found to hold for a variety of M_{thres} a few days up to one week before the strong EQ occurrence [6, 30, 40, 41, 44–47, 55, 59] . This is very important from practical point of view because it enables the estimation of the occurrence time of a strong EQ with an accuracy of one week, or so.

The entropy S in natural time is defined[6, 35, 39, 54, 60] by the relation

$$S = \sum_{k=1}^{N} p_k \chi_k \ln \chi_k - \left(\sum_{k=1}^{N} p_k \chi_k \right) \ln \left(\sum_{m=1}^{N} p_m \chi_m \right). \quad (4)$$

It is a dynamic entropy showing [61] positivity, concavity and Lesche [62, 63] experimental stability. When Q_k are independent and identically-distributed random variables, S approaches[60] the value $S_u \equiv \frac{\ln 2}{2} - \frac{1}{4} \approx 0.0966$ that corresponds to the case $Q_k = 1/N$, which within the context of natural time is usually termed "uniform" distribution [6, 39, 54]. Notably, S changes its value to S_- upon time-reversal, i.e., when the first event becomes last ($Q_1 \to Q_N$), the second last but one ($Q_2 \to Q_{N-1}$) etc,

$$S_- = \sum_{k=1}^{N} p_{N-k+1} \chi_k \ln \chi_k - \left(\sum_{k=1}^{N} p_{N-k+1} \chi_k \right) \ln \left(\sum_{m=1}^{N} p_{N-m+1} \chi_m \right), \quad (5)$$

and hence it gives us the possibility to observe the (true) time-arrow[61]. Interestingly, it has been established [6, 54] that both S and S_- for SES activities are smaller than S_u,

$$S, S_- \leq S_u. \quad (6)$$

On the other hand, these conditions are violated for a variety of similar looking electrical noises (e.g. see Table 4.6 on p. 228 of Ref. [6]).

Natural time has been recently employed by Turcotte and coworkers[64–67] as a basis for a new method to estimate the current level of seismic risk called "earthquake nowcasting". This will be explained in the next Section.

III. RESULTS

A. Geoelectric field changes

Figure 2 depicts an SES activity that was recorded in PIR station (see Fig.1), which comprises a multitude of measuring dipoles, on 2 October 2018 between 04:20 and 05:05 UTC. The potential differences ΔV of three of these electric dipoles of comparable length L (a few km) deployed in the NEE direction are shown. The true headings of these dipoles are from top to bottom in Fig.2 are 75.48^o, 64.83^o, and 76.16^o. An inspection of this figure reveals that the SES activity resembles a telegraph signal with periods of activity and periods of inactivity as it is usually the case [36, 38, 39]. If we impose a threshold in the ΔV variation[36, 38, 39], we can obtain the dichotomous (0-1) representation of the SES activity depicted by the cyan color in Fig.2.

B. Natural time analysis of geoelectrical signals. Criteria for distinguishing SES

Apart from the aforementioned $\Delta V/L$ criterion suggested long ago for the distinction of SES from man-made noise [9], natural time analysis has provided, as mentioned, three additional criteria for the classification of an electric signal as SES activity. These criteria are Eq.(3) and the conditions (6). The analysis in natural time of the dichotomous representation shown in Fig.2 results in $\kappa_1 = 0.072(2)$, $S = 0.066(2)$ and $S_- = 0.079(3)$, which are obviously compatible with the criteria for distinguishing SES from noise. This leads us to support that the anomalous variation of the electric field of the Earth observed on 2 October 2018 is indeed an SES activity.

C. Estimation of the occurrence time of the impending EQ

We now follow the method suggested in Ref.[30] for the estimation of the occurrence time of the impending strong EQ by analyzing in natural time all the small EQs of magnitude greater than or equal to M_{thres} that occurred after the initiation of the SES activity recorded on 2 October 2018 within the selectivity map of PIR measuring station shown by the gray shaded area in Fig.1. The EQ catalog[68] of the Institute of Geodynamics of the National Observatory of Athens has been used and

each time a new small EQ takes place we calculate the κ_1 values corresponding to the events that occurred within all the possible subareas of the PIR selectivity map that include this EQ [30]. This procedure leads to an ensemble of κ_1 values from which we can calculate the probability Prob(κ_1) of κ_1 to lie within $\kappa_1 \pm 0.025$. Figures 3(a), (b), (c), and (d) depict the histograms of Prob(κ_1) obtained after the occurrence of each small EQ with magnitude ML(ATH) [9, 10] greater than or equal to M_{thres}=2.7, 2.8, 2.9, and 3.0, respectively. We observe that within a period of 5 hours around 18 October 2018 00:30 UTC all the four distributions Prob(κ_1) exhibit a maximum at $\kappa_1 = 0.070$. This behavior has been found, as already mentioned, to occur a few days up to one week or so before the strong EQ occurrence [6, 30, 45–47]. Actually, one week later, i.e., on 25 October 2018, a strong M_w6.8 EQ occured[1] within the selectivity map of the PIR measuring station (see the red star in Fig.1). Interestingly, as it is written in the legends of the panels of Fig.3, two of the three small EQs that led to the fulfillment of the criticality condition $\kappa_1 = 0.070$ originated from epicentral areas located only 20 or 25km south from that of the strong EQ.

D. Estimation of the current level of risk by applying EQ nowcasting

Nowcasting EQs is a recent method for the determination of the current state of a fault system and the estimation of the current progress in the EQ cycle[64]. It uses a global EQ catalog to calculate from "small" EQs the level of hazard for "large" EQs. This is achieved by employing the natural time concept and count the number n_s of "small" EQs that occur after a "strong" EQ. The current value $n(t)$ of n_s since the occurrence of the last "strong" EQ is compared with the cumulative distribution function (cdf) $P(n_s < n(t))$ of n_s obtained when ensuring that we have enough data to span at least 20 or more "large" EQ cycles. The EQ potential score (EPS) which equals the "current" cdf value, EPS=$P(n_s < n(t))$ is therefore a unique measure of the current level of hazard and assigns a number between 0% and 100% to every region so defined. Nowcasting EQs has already found many useful applications[65–67] among which is the estimation of seismic risk to Global Megacities. For this application[65] the EQs with depths smaller than a certain value D within a larger area are studied in order to obtain the cdf $P(n_s < n(t))$. Then the number $\tilde{n}_s$ of "small" EQs around a Megacity, e.g., EQs in a circular region of epicentral distances smaller than a radius R with hypocenters shallower than D, is counted since the occurrence of the last "strong" EQ in this region. Based on the ergodicity of EQs that has been proven[69–71] by using the metric published in Refs.[72, 73], Rundle et al. [65] suggested that the seismic risk around a Megacity can be estimated by using the EPS corresponding to the current $\tilde{n}_s$ estimated in the circular region. Especially

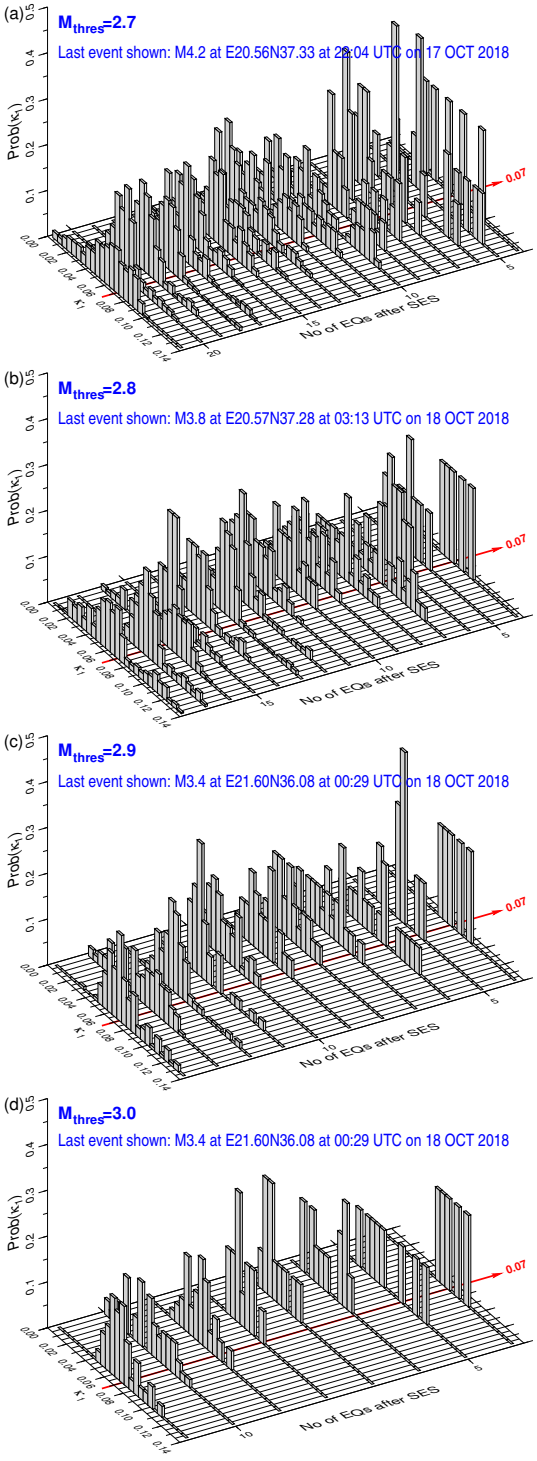


FIG. 3: (color online) (a) to (d): The probability distribution Prob(κ_1) of κ_1 versus κ_1 as it results after the occurrence of each small EQ within the selectivity area of PIR (see the gray shaded area in Fig. 1) for various magnitude thresholds M_{thres}=2.7, 2.8, 2.9, and 3.0.

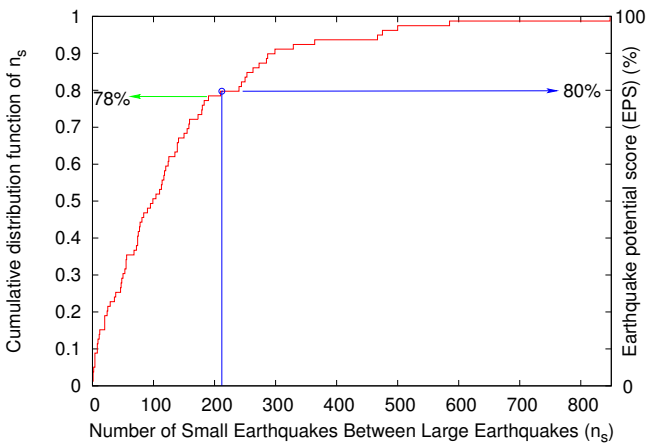


FIG. 4: (color online)Estimation of the EQ potential score (EPS) based on the cumulative distribution function of the number n_s of the small EQs ($6.0 > M \geq 4.0$) that occur within the large area $N_{29}^{47}E_{12}^{35}$ depicted in Fig.1 between the occurrence of two strong ($M \geq 6.0$) EQs. The number $\tilde{n}_s$ of small EQs that occurred within $R \leq 225$km with depths $D \leq 200$km from the city of Patras: (i)since the M_w6.5 EQ on 17 November 2015 07:11 UTC [75] and before the occurrence of the M_w6.8 EQ on 25 October 2018 was 212 (see the blue lines for EPS) and (ii)since the occurrence of the latter EQ on 25 October 2018 until 19 January 2019 is 205 (see the green line for EPS).

in their Fig.2, they used the large area $N_{29}^{47}E_{12}^{35}$ in order to estimate the EPS for EQs of magnitude greater than or equal to 6.5 at an area of radius $R = 400km$ around the capital of Greece Athens. Figure 4 shows the results of a similar calculation based on the United States National EQ Information Center PDE catalog (the data of which are available from Ref.[74]) which we performed focusing on the city of Patras, Greece, for EQs of magnitude greater than or equal to 6.0. Notably before the occurrence of the M_w6.8 EQ on 25 October 2018 EPS was found to be as high as 80%, see the blue lines in Fig. 4. A similar calculation since the occurrence of the latter M_w6.8 EQ until 19 January 2019 leads to $\tilde{n}_s = 205$ resulting in EPS 78% (see the green line in Fig. 4).

IV. DISCUSSION

Recently, the statistical significance of the Earth's electric and magnetic field variations preceding EQs has been studied[76] on the basis of the modern tools of event coincidence analysis[77–79] and receiver operating characteristics[80, 81]. Using an SES dataset[9, 10, 82] from 1980s it was found that SES are statistically significant precursors to EQs for lead times in the following four distinct time periods: 3 to 9 days, 18 to 24 days, 43 to 47 days, and 58 to 62 days (the first one corresponds to single SES, while the latter three to SES activities [76]). Since the SES activity, shown in Fig.2, was recorded on 2 October 2018, the SES lead time for the present case of the M_w6.8 EQ on 25 October 2018, which is 23 days, favorably falls within the second time period of 18 to 24 days. Moreover, the analysis of the seismicity subsequent to the initiation of the SES activity in the selectivity area of the PIR station has led to the conclusion that the criticality condition $\kappa_1 = 0.070$ has been satisfied early in the morning on 18 October 2018. This compares favorably with the time window of a few days up to one week already found from various SES activities in Greece, Japan and United States [6, 30, 45–47, 59].

Let us now turn to the results concerning the entropy of the SES activity of Fig.2 in natural time. As it was reported both S and S_- are well below S_u in accordance with the findings (e.g. see Ref. [54]) so far for SES activities. Based on the critical properties that characterize the emission of signals that precede rupture (i.e., infinite range correlations compatible with a detrended fluctuation analysis (DFA)[83–85] exponent $\alpha_{DFA} = 1$) a fractional Brownian motion [86, 87] model has been suggested[41] according to which both S and S_- values should scatter around 0.079 with a standard deviation of 0.011 (see Fig.4 of Ref.[41]). Interestingly, the values $S = 0.066(2)$ and $S_- = 0.079(3)$ of the SES activity recorded on 2 October 2018 are fully compatible with this model.

Finally, the successful results (i.e., the 80% EPS found before the occurrence of the M_w6.8 EQ on 25 October 2018) from the EQ nowcasting method which is based on natural time are very promising. Nowcasting does not involve any model and there are no free parameters to be fit to the data [64].

On 3 January 2019, an electrical activity (Fig.5) was recorded at PAT measuring station (close to the city of Patras see Fig.1) which was classified as an SES activity because its natural time analysis by using the procedure described in Ref.[43] resulted in $\kappa_1 = 0.075(22)$, $S = 0.071(22)$, and $S_- = 0.075(30)$. Similar conclusion was drawn for an electrical activity recorded at PIR on 9 January 2019. To estimate the occurrence time of the impending EQ, we currently analyze in natural time (as in subsection III.C) the subsequent seismic activity occurring within the area comprising the gray shaded area of Fig.1 and the one around PAT (in view of the green line in Fig.4, see also the rectangle with solid lines in Fig.8 of Ref.[30]) [88, 89].

V. SUMMARY AND CONCLUSIONS

The strong EQ of magnitude M_w6.8 that occurred in Western Greece on 25 October 2018 was preceded by an SES activity on 2 October 2018 recorded at PIR measuring station of VAN telemetric network. The EQ epicenter was located within the selectivity map of PIR depicted by the gray shaded area in Fig.1.

The lead time of 23 days between the precursory SES activity and the strong EQ is statistically significant as

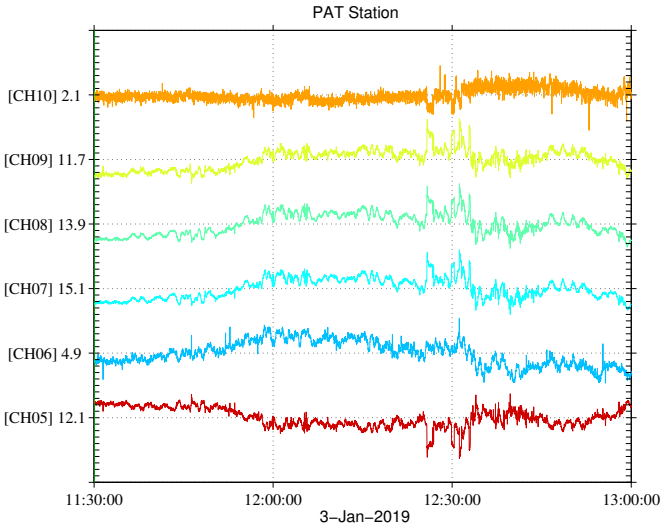


FIG. 5: (color online) The SES activity on 3 January 2019 at PAT measuring station recorded on a multitude of electric dipoles labeled CH05 to CH10. The numbers on the left vertical axis denote the scale of the variation of the potential difference in mV per division for each dipole.

recently found by the recent methods of event coincidence analysis and receiver operating characteristics. Both the entropy S and the entropy S_- under time reversal in natural time are compatible with previous observation for SES activities as well as agree with a model for SES activities based on fractional Brownian motion. The analysis in natural time of the seismicity subsequent to the SES activity by considering the events occurring within the selectivity area of PIR shows that criticality has been reached early morning on 18 October 2018, almost a week before the strong EQ occurrence in accordance with the earlier findings. When employing the recent method of nowcasting earthquakes, which is based on natural time, we find an earthquake potential score around 80% just before the occurrence of the M_w6.8 earthquake on 25 October 2018. Here, we also report the recording of more recent SES activities at PIR and PAT [88–91].

[1] United States Geological Survey, Earthquake Hazards Program (2018), `https://earthquake.usgs.gov/earthquakes/eventpage/us1000hhb1/technical`.

[2] United States Geological Survey, Earthquake Hazards Program (2018), `https://earthquake.usgs.gov/earthquakes/eventpage/us1000hhay/technical`.

[3] S. Uyeda, E. Al-Damegh, E. Dologlou, and T. Nagao, Tectonophysics **304**, 41 (1999).

[4] P. Varotsos, K. Eftaxias, M. Lazaridou, K. Nomicos, N. Sarlis, N. Bogris, J. Makris, G. Antonopoulos, and J. Kopanas, Acta Geophysica Polonica **44**, 301 (1996).

[5] P. Varotsos, *The Physics of Seismic Electric Signals* (TERRAPUB, Tokyo, 2005).

[6] P. A. Varotsos, N. V. Sarlis, and E. S. Skordas, *Natural Time Analysis: The new view of time. Precursory Seismic Electric Signals, Earthquakes and other Complex Time-Series* (Springer-Verlag, Berlin Heidelberg, 2011).

[7] P. Varotsos and K. Alexopoulos, Tectonophysics **110**, 73 (1984).

[8] P. Varotsos and K. Alexopoulos, Tectonophysics **110**, 99 (1984).

[9] P. Varotsos and M. Lazaridou, Tectonophysics **188**, 321 (1991).

[10] P. Varotsos, K. Alexopoulos, and M. Lazaridou, Tectonophysics **224**, 1 (1993).

[11] P. A. Varotsos, N. V. Sarlis, E. S. Skordas, and M. S. Lazaridou, J. Appl. Phys. **103**, 014906 (2008).

[12] S. Uyeda, T. Nagao, Y. Orihara, T. Yamaguchi, and I. Takahashi, Proc. Natl. Acad. Sci. USA **97**, 4561 (2000).

[13] S. Uyeda, M. Hayakawa, T. Nagao, O. Molchanov, K. Hattori, Y. Orihara, K. Gotoh, Y. Akinaga, and H. Tanaka, Proc. Natl. Acad. Sci. USA **99**, 7352 (2002).

[14] Y. Orihara, M. Kamogawa, T. Nagao, and S. Uyeda, Proc. Natl. Acad. Sci. U.S.A. **109**, 19125 (2012).

[15] J. Zlotnicki, V. Kossobokov, and J.-L. Le Mouël, Tectonophysics **334**, 259 (2001).

[16] Q. Huang, Journal of Asian Earth Sciences **41**, 421 (2011).

[17] S. D. Gao, J. Tang, X. B. Du, X. F. Liu, Y. G. Su, Y. P. Chen, G. R. Di, D. L. Mei, Y. Zhan, and L. F. Wang, Chinese J. Geophys. **53**, 512 (2010).

[18] Y.-Y. Fan, X.-B. Du, J. Zlotnicki, D.-C. Tan, Z.-H. An, J.-Y. Chen, G.-L. Zheng, J. Liu, and T. Xie, Chinese J. Geophys. **53**, 997 (2010).

[19] A. Ramírez-Rojas, E. L. Flores-Márquez, L. Guzmán-Vargas, G. Gálvez-Coyt, L. Telesca, and F. Angulo-Brown, Nat. Hazards Earth Syst. Sci. **8**, 1001 (2008).

[20] A. Ramírez-Rojas, L. Telesca, and F. Angulo-Brown, Nat. Hazards Earth Syst. Sci. **11**, 219 (2011).

[21] N. V. Sarlis, P. A. Varotsos, E. S. Skordas, J. Zlotnicki, T. Nagao, A. Rybin, M. S. Lazaridou-Varotsos, and K. Papadopoulou, Earthquake Science **31**, 44 (2018).

[22] P. Varotsos and K. Alexopoulos, *Thermodynamics of Point Defects and their Relation with Bulk Properties* (North Holland, Amsterdam, 1986).

[23] P. Varotsos and D. Miliotis, Journal of Physics and Chemistry of Solids **35**, 927 (1974).

[24] M. Lazaridou, C. Varotsos, K. Alexopoulos, and P. Varotsos, J. Phys. C: Solid State **18**, 3891 (1985).

[25] P. Varotsos, Solid State Ionics **179**, 438 (2008).

[26] P. Varotsos and K. Alexopoulos, Tectonophysics **136**, 335 (1987).

[27] P. Varotsos, M. Lazaridou, K. Eftaxias, G. Antonopoulos, J. Makris, and J. Kopanas, in *The Critical Review of VAN: Earthquake Prediction from Seismic Electric Signals*, edited by S. J.Lighthill (World Scientific, Singapore, 1996), pp. 29–76.

[28] M. S. Lazaridou-Varotsos, *Earthquake Prediction by Seis-*

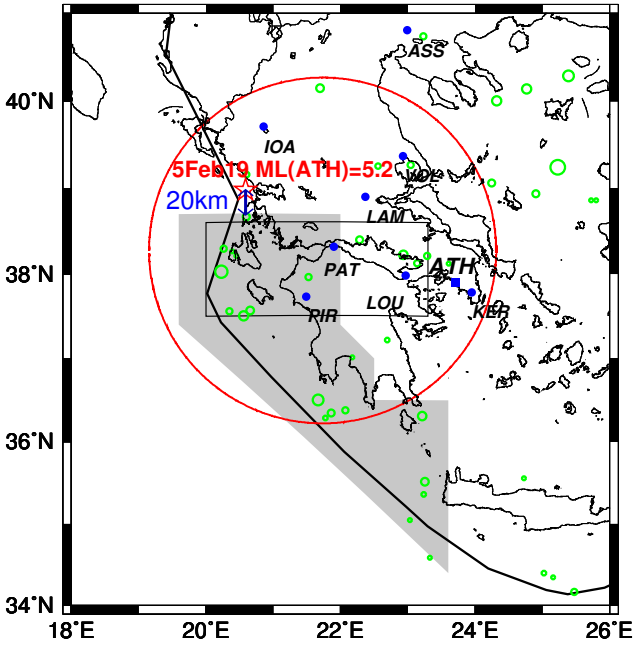


FIG. 6: Map depicting the epicenter (red star) of the ML(ATH)=5.2 EQ on 5 February 2019 located very close to the NorthWestern edge of the PIR selectivity map.

mic Electric Signals: The success of the VAN method over thirty years (Springer Praxis Books, Berlin Heidelberg, 2013).

[29] S. Uyeda, in *The Critical Review of VAN: Earthquake Prediction from Seismic Electric Signals*, edited by S. J. Lighthill (World Scientific, Singapore, 1996), vol. 16, pp. 3–28.

[30] N. V. Sarlis, E. S. Skordas, M. S. Lazaridou, and P. A. Varotsos, Proc. Jpn. Acad. Ser. B Phys. Biol. Sci. **84**, 331 (2008).

[31] P. Varotsos, N. Sarlis, M. Lazaridou, and P. Kapiris, J. Appl. Phys. **83**, 60 (1998).

[32] N. Sarlis, M. Lazaridou, P. Kapiris, and P. Varotsos, Geophys. Res. Lett. **26**, 3245 (1999).

[33] P. Varotsos, N. Sarlis, and M. Lazaridou, Acta Geophysica Polonica **48**, 141 (2000).

[34] P. Varotsos, N. Sarlis, and E. Skordas, Acta Geophysica Polonica **48**, 263 (2000).

[35] P. A. Varotsos, N. V. Sarlis, and E. S. Skordas, Practica of Athens Academy **76**, 294 (2001), `http://physlab.phys.uoa.gr/org/pdf/p3.pdf`.

[36] P. A. Varotsos, N. V. Sarlis, and E. S. Skordas, Phys. Rev. E **66**, 011902 (2002).

[37] P. A. Varotsos, N. V. Sarlis, and E. S. Skordas, Acta Geophysica Polonica **50**, 337 (2002).

[38] P. A. Varotsos, N. V. Sarlis, and E. S. Skordas, Phys. Rev. E **67**, 021109 (2003).

[39] P. A. Varotsos, N. V. Sarlis, and E. S. Skordas, Phys. Rev. E **68**, 031106 (2003).

[40] P. A. Varotsos, N. V. Sarlis, H. K. Tanaka, and E. S. Skordas, Phys. Rev. E **72**, 041103 (2005).

[41] P. A. Varotsos, N. V. Sarlis, E. S. Skordas, H. K. Tanaka, and M. S. Lazaridou, Phys. Rev. E **73**, 031114 (2006).

[42] P. A. Varotsos, N. V. Sarlis, E. S. Skordas, H. K. Tanaka, and M. S. Lazaridou, Phys. Rev. E **74**, 021123 (2006).

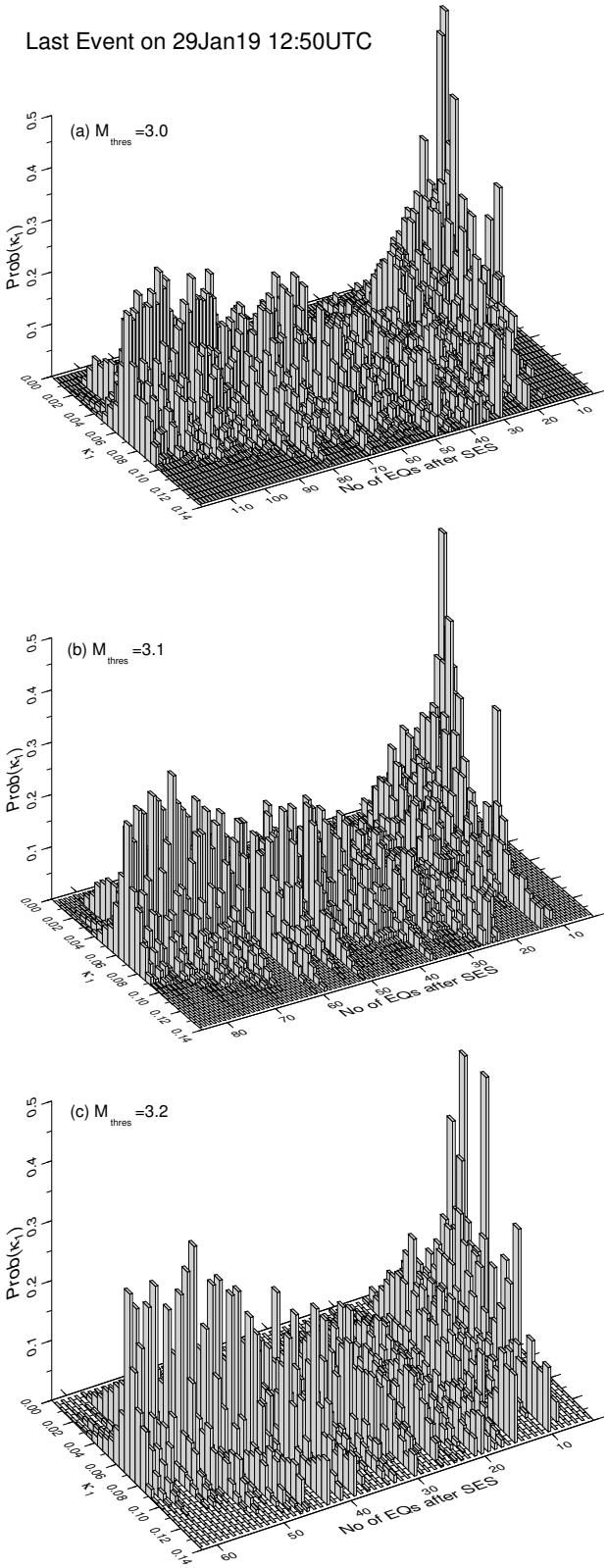


FIG. 7: (color online) (a) to (c): The probability distribution Prob(κ_1) of κ_1 versus κ_1 as it results after the occurrence of each small EQ within the selectivity map of PIR (see the gray shaded area in Fig. 1) for various magnitude thresholds M_{thres}=3.0, 3.1, and 3.2 after the SES activity at PIR on 9 January 2019. The last event considered is the ML(ATH)=3.5 EQ at 12:50 UTC on 29 January 2019 at 37.13^{o}N 20.59^{o}E.

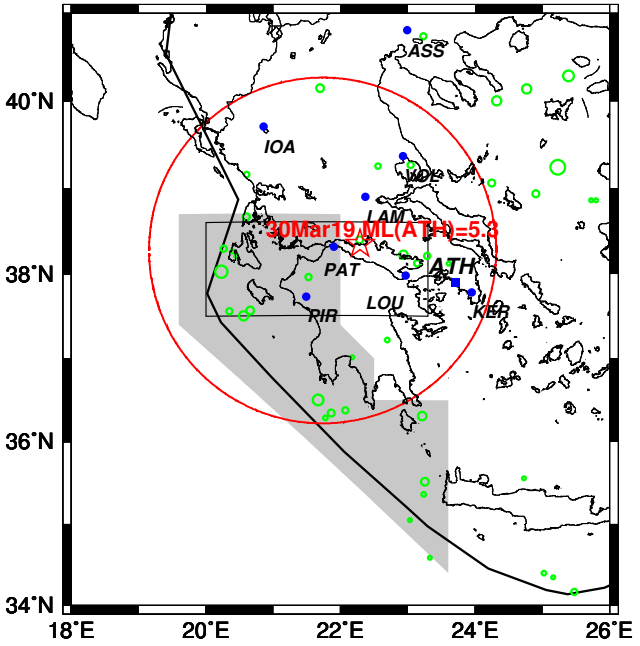


FIG. 8: Map depicting the epicenter (red star) of the ML(ATH)=5.3 EQ on 30 March 2019 located inside the PAT selectivity map (depicted by black rectangle which reproduces the rectangle with solid lines in Fig.8 of Ref.[30] mentioned in Section IV) at a distance around 30km from the measuring station (PAT).

[43] P. A. Varotsos, N. V. Sarlis, and E. S. Skordas, Chaos **19**, 023114 (2009).
[44] P. A. Varotsos, N. V. Sarlis, E. S. Skordas, and M. S. Lazaridou, Appl. Phys. Lett. **91**, 064106 (2007).
[45] P. A. Varotsos, N. V. Sarlis, E. S. Skordas, S. Uyeda, and M. Kamogawa, EPL **92**, 29002 (2010).
[46] P. A. Varotsos, N. V. Sarlis, E. S. Skordas, S.-R. G. Christopoulos, and M. S. Lazaridou-Varotsos, Earthquake Science **28**, 215 (2015).
[47] P. A. Varotsos, N. V. Sarlis, and E. S. Skordas, Earthquake Science **30**, 209 (2017).
[48] N. V. Sarlis, E. S. Skordas, P. A. Varotsos, T. Nagao, M. Kamogawa, H. Tanaka, and S. Uyeda, Proc. Natl. Acad. Sci. USA **110**, 13734 (2013).
[49] N. V. Sarlis, E. S. Skordas, P. A. Varotsos, T. Nagao, M. Kamogawa, and S. Uyeda, Proc. Natl. Acad. Sci. USA **112**, 986 (2015).
[50] P. A. Varotsos, N. V. Sarlis, E. S. Skordas, and M. S. Lazaridou, Tectonophysics **589**, 116 (2013).
[51] P. A. Varotsos, N. V. Sarlis, and E. S. Skordas, J. Geophys. Res.: Space Physics **119**, 9192 (2014).
[52] N. V. Sarlis and E. S. Skordas, Entropy **20**, 882 (2018).
[53] H. Kanamori, Nature **271**, 411 (1978).
[54] N. V. Sarlis, Entropy **19**, 177 (2017).
[55] P. Varotsos, N. V. Sarlis, E. S. Skordas, S. Uyeda, and M. Kamogawa, Proc. Natl. Acad. Sci. USA **108**, 11361 (2011).
[56] M. Hayakawa, A. Schekotov, S. Potirakis, and K. Eftaxias, Proc. Jpn Acad. Ser. B Phys. Biol. Sci. **91**, 25 (2015).
[57] S. M. Potirakis, T. Asano, and M. Hayakawa, Entropy **20**, 199 (2018).
[58] S. M. Potirakis, A. Schekotov, T. Asano, and

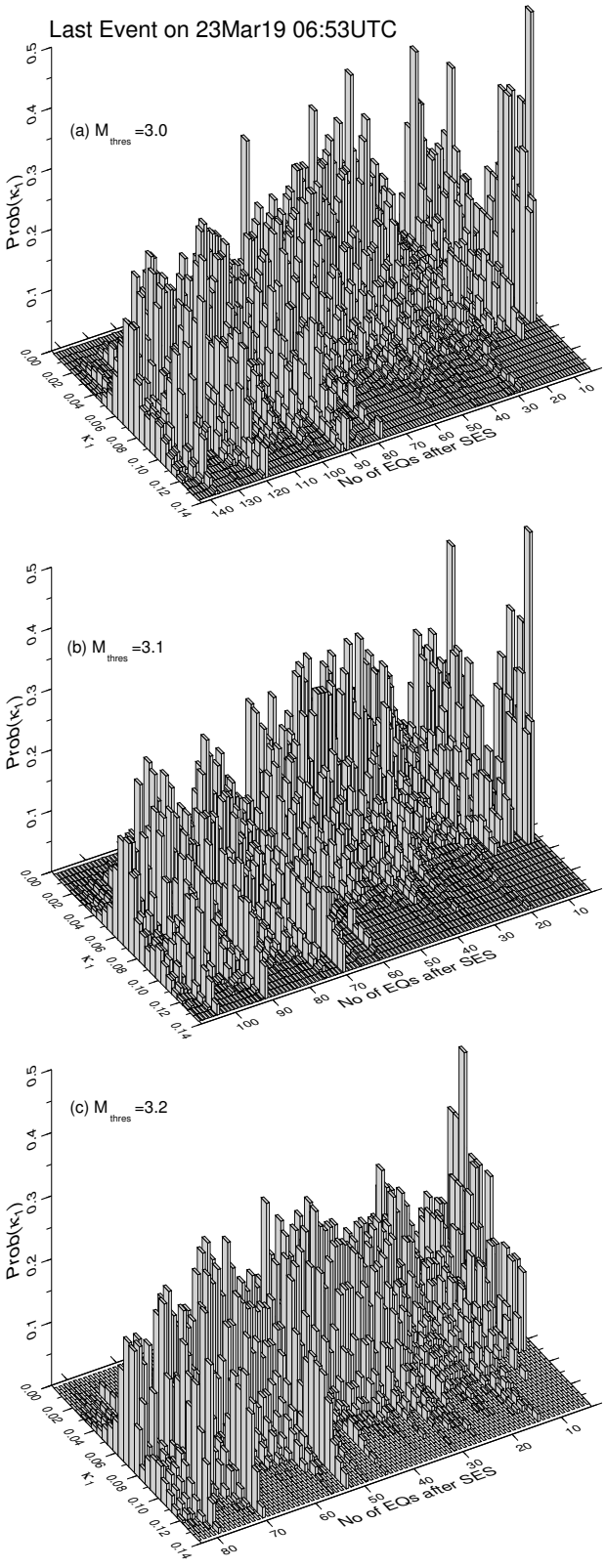


FIG. 9: (color online) (a) to (c): The probability distribution Prob(κ_1) of κ_1 versus κ_1 as it results after the occurrence of each small EQ within the selectivity map of PAT (see the black rectangle in Fig. 8) for various magnitude thresholds M_{thres}=3.0, 3.1, and 3.2 after the SES activity at PAT on 3 January 2019. The last event considered is the ML(ATH)=3.2 EQ at 6:53 UTC on 23 March 2019 at 37.69^{o}N 20.61^{o}E.

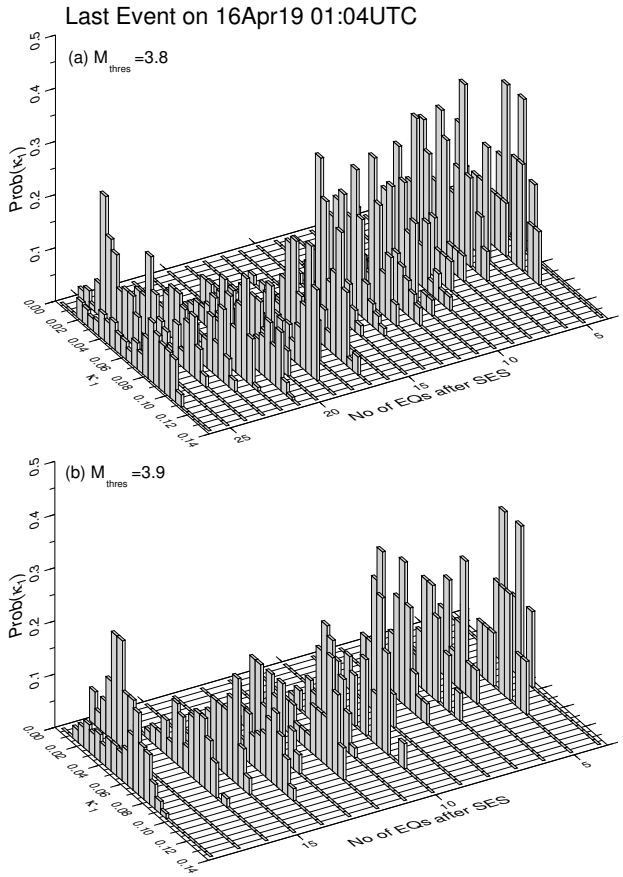


FIG. 10: (color online) The probability distribution Prob(κ_1) of κ_1 versus κ_1 as it results after the occurrence of each small EQ within the selectivity map of PAT (see the black rectangle in Fig. 8) for the magnitude thresholds (a)$M_{\rm thres}$=3.8 and (b)$M_{\rm thres}$=3.9 after the SES activity at PAT on 3 January 2019. The last event considered is the ML(ATH)=3.9 EQ at 1:04 UTC on 16 April 2019 at 37.71^{o}N 20.71^{o}E.

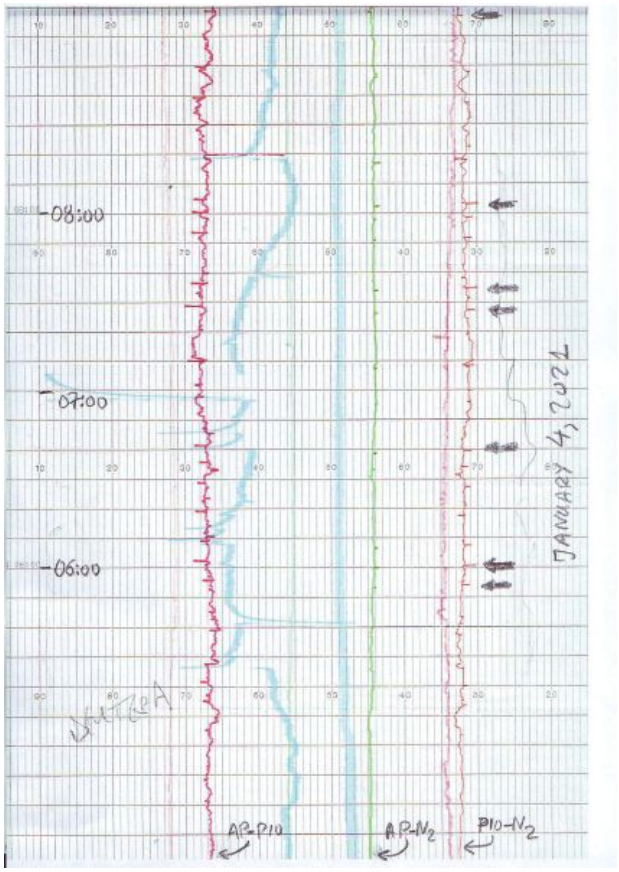


FIG. 11: (color online) An excerpt of the raw data recordings at the central station of the telemetric network for the PAT geoelectric station on 4 January 2021. The thick arrows show the most evident SES pulses at the three long measuring dipoles labeled AP-PIO, AP-N_2, and PIO-N_2.

M. Hayakawa, Journal of Asian Earth Sciences **154**, 419 (2018).

[59] S. Uyeda, M. Kamogawa, and H. Tanaka, J. Geophys. Res. **114**, B02310 (2009).

[60] P. A. Varotsos, N. V. Sarlis, E. S. Skordas, and M. S. Lazaridou, Phys. Rev. E **70**, 011106 (2004).

[61] P. A. Varotsos, N. V. Sarlis, H. K. Tanaka, and E. S. Skordas, Phys. Rev. E **71**, 032102 (2005).

[62] B. Lesche, J. Stat. Phys. **27**, 419 (1982).

[63] B. Lesche, Phys. Rev. E **70**, 017102 (2004).

[64] J. B. Rundle, D. L. Turcotte, A. Donnellan, L. Grant Ludwig, M. Luginbuhl, and G. Gong, Earth and Space Science **3**, 480 (2016).

[65] J. B. Rundle, M. Luginbuhl, A. Giguere, and D. L. Turcotte, Pure and Applied Geophysics **175**, 647 (2018).

[66] M. Luginbuhl, J. B. Rundle, A. Hawkins, and D. L. Turcotte, Pure and Applied Geophysics **175**, 49 (2018).

[67] M. Luginbuhl, J. B. Rundle, and D. L. Turcotte, Pure and Applied Geophysics **175**, 661 (2018).

[68] National Observatory of Athens, Institute of Geodynamics (2018), `http://www.gein.noa.gr/en/seismicity/recent-earthquakes`.

[69] C. D. Ferguson, W. Klein, and J. B. Rundle, Phys. Rev. E **60**, 1359 (1999).

[70] K. F. Tiampo, J. B. Rundle, W. Klein, J. S. S. Martins, and C. D. Ferguson, Phys. Rev. Lett. **91**, 238501 (2003).

[71] K. F. Tiampo, J. B. Rundle, W. Klein, J. Holliday, J. S. Sá Martins, and C. D. Ferguson, Phys. Rev. E **75**, 066107 (2007).

[72] D. Thirumalai, R. D. Mountain, and T. R. Kirkpatrick, Phys. Rev. A **39**, 3563 (1989).

[73] R. D. Mountain and D. Thirumalai, Phys. Rev. A **45**, R3380 (1992).

[74] United States Geological Survey, Earthquake Hazards Program (2018), `https://earthquake.usgs.gov/earthquakes/eventpage/us1000hhb1/technical`.

[75] United States Geological Survey, Earthquake Hazards Program (2015), `https://earthquake.usgs.gov/earthquakes/eventpage/us10003ywp/technical`.

[76] N. V. Sarlis, Entropy **20**, 561 (2018).

[77] J. Donges, C.-F. Schleussner, J. Siegmund, and R. Donner, The European Physical Journal Special Topics **225**, 471 (2016), ISSN 1951-6401.

[78] C.-F. Schleussner, J. F. Donges, R. V. Donner, and H. J. Schellnhuber, Proc. Natl. Acad. Sci. USA **113**, 9216 (2016).

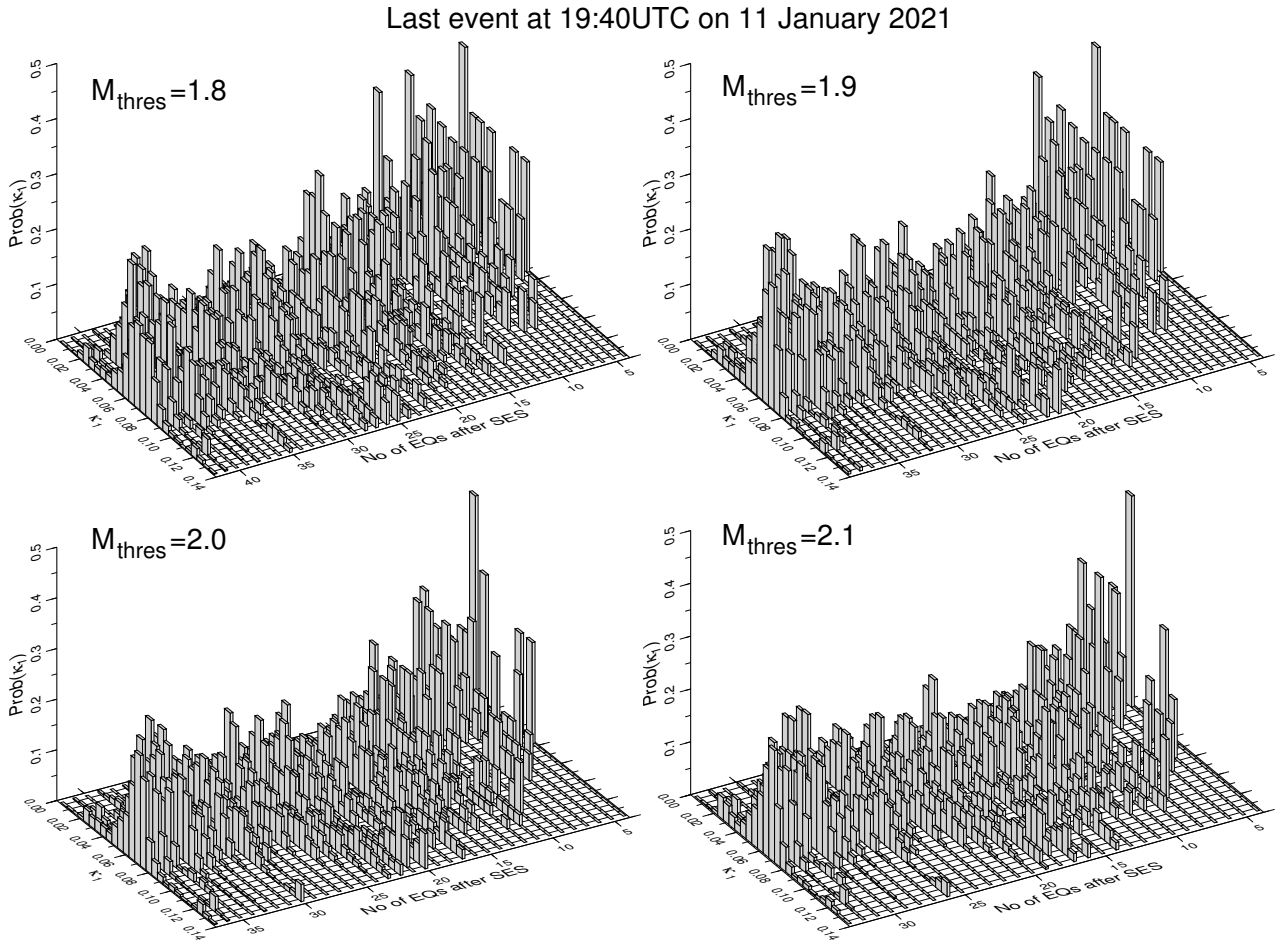


FIG. 12: The probability distribution Prob(κ_1) of κ_1 versus κ_1 as it results after the occurrence of each small EQ within the selectivity map of PAT (see the black rectangle in Fig. 8) for various low magnitude thresholds after the SES activity at PAT on 4 January 2021. The last event considered is the ML(ATH)=2.6 EQ at 19:40 UTC on 11 January 2021 at 38.39^{o}N 22.01^{o}E.

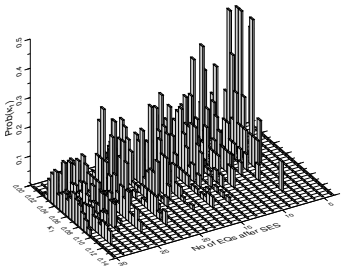


FIG. 13: The probability distribution Prob(κ_1) of κ_1 versus κ_1 as it results after the occurrence of each small EQ within the selectivity map of PAT (see the black rectangle in Fig. 8) for magnitude threshold M_{thres} = 3.2 after the SES activity at PAT on 4 January 2021. The last event considered is the ML(ATH)=3.2 EQ at 02:37 UTC on 17 February 2021 at 38.35^{o}N 21.94^{o}E.

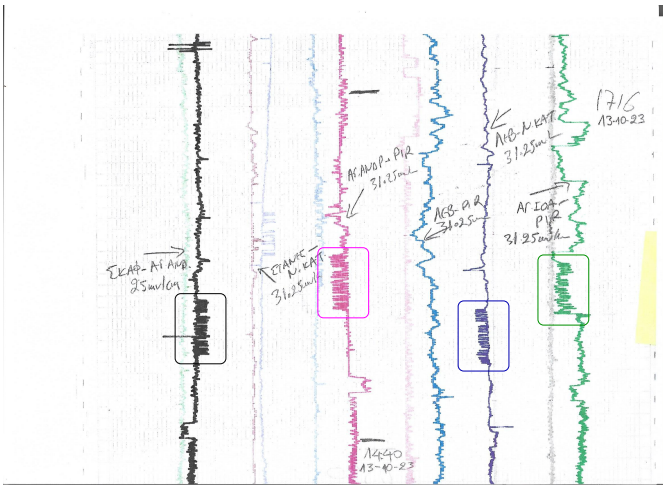


FIG. 14: An excerpt of the raw data recordings at the central station of the telementric network for the Pirgos (PIR) station on 13 October 2023. The simultaneous raw data recordings at four channels are surrounded by the relevant colored rectangles.

[79] J. F. Siegmund, N. Siegmund, and R. V. Donner, Computers & Geosciences **98**, 64 (2017), ISSN 0098-3004.
[80] T. Fawcett, Pattern Recogn. Lett. **27**, 861 (2006).
[81] N. V. Sarlis and S.-R. G. Christopoulos, Comput. Phys.

Commun. **185**, 1172 (2014).

[82] E. Dologlou, Tectonophysics **224**, 189 (1993), ISSN 0040-1951.

[83] C.-K. Peng, S. V. Buldyrev, S. Havlin, M. Simons, H. E. Stanley, and A. L. Goldberger, Phys. Rev. E **49**, 1685 (1994).

[84] C. K. Peng, S. V. Buldyrev, A. L. Goldberger, S. Havlin, R. N. Mantegna, M. Simons, and H. E. Stanley, Physica A **221**, 180 (1995).

[85] J. W. Kantelhardt, E. Koscielny-Bunde, H. H. A. Rego, S. Havlin, and A. Bunde, Physica A **295**, 441 (2001).

[86] B. B. Mandelbrot and J. W. van Ness, SIAM Rev. **10**, 422 (1968).

[87] B. B. Mandelbrot and J. R. Wallis, Water Resources Research **5**, 321 (1969).

[88] *Note added on 17 April 2019.* The following two EQs with ML(ATH)> 5.0 occurred so far: First, the ML(ATH)=5.2 (Mww=5.4 see `https://earthquake.usgs.gov/earthquakes/eventpage/us2000jdgj/moment-tensor?source=us&code=us_2000jdgj_mww`) EQ at 02:26 UTC on 5 February 2019 with an epicenter at 38.98^{o}N 20.59^{o}E lying very close to the NorthWestern edge of the PIR selectivity map, see Fig.6. It occurred almost one week after the criticality condition $\kappa_1 = 0.070$ has been fulfilled (see Fig.7) exhibiting magnitude threshold invariance when analyzing the seismicity within the PIR selectivity map after the SES activity on 9 January 2019. Second, the ML(ATH)=5.3 (Mww=5.3 see `https://earthquake.usgs.gov/earthquakes/eventpage/us2000k7ki/moment-tensor?source=us&code=us_2000k7ki_mww`) EQ at 10:46 UTC on 30 March 2019 with an epicenter at 38.35^{o}N 22.29^{o}E lying inside the PAT selectivity map (Fig.8) at a distance around 30km from the measuring station. It occurred almost one week after the criticality condition $\kappa_1 = 0.070$ has been fulfilled (see Fig.9) exhibiting magnitude threshold invariance when analyzing the seismicity within the PAT selectivity map after the SES activity on 3 January 2019. The study still continues and upon the occurrence of the ML(ATH)=3.9 EQ at 1:04 UTC on 16 April 2019 with an epicenter at 37.71^{o}N 20.71^{o}E, we find that Prob(κ_1) maximizes at $\kappa_1 = 0.070$ for M_{thres}=3.9, see Fig.10(b). The study of Prob(κ_1) was extended for other values of M_{thres} and revealed that a secondary peak of Prob(κ_1) appears at $\kappa_1 = 0.070$ for M_{thres}=3.8, see Fig.10(a).

[89] *Note added on 20 June 2019.* Our previous Note has been followed by a ML(ATH)=4.7 or Ms(ATH)=5.2 EQ that occurred at 16:57 UT on 13 May 2019 with an epicenter at 37.68^{o}N 21.77^{o}E lying inside the PAT selectivity map (Fig. 8) accompanied by several other smaller EQs in the same region.

[90] *Note added on 24 January 2021.* Following the policy described in the introduction of Section 7.2 of Ref.[6], we report that on 4 January 2021 an SES activity comprising a large number of SES pulses (lasting from 05:00 until around 12:30 UTC) was recorded at PAT, an excerpt of the raw data of which is depicted in Fig.11. To estimate the occurrence time of the impending EQ we analyzed in natural time the subsequent seismic activity occurring within the PAT selectivity map depicted by the rectangle with the solid black line in Fig.8. The results depicted in Fig.12 for four low magnitude thresholds M_{thres}=1.8, 1.9, 2.0, and 2.1 show that the criticality condition $\kappa_1 = 0.070$ was satisfied upon the occurrence of the ML(ATH)=2.6 EQ at 19:40 UTC on 11 January 2021 at 38.39^{o}N 22.01^{o}E almost one day before the ML(ATH)=4.8 or Ms(ATH)=5.3 EQ at 22:10 UTC on 12 January 2021 with an epicenter at 38.40^{o}N 22.05^{o}E (according to USGS, Mww=5.2 see `https://earthquake.usgs.gov/earthquakes/eventpage/us6000d7vr/technical`). We currently investigate whether the criticality condition will be obeyed again, but for larger magnitude thresholds.

[91] *Note added on 17 February 2021.* Today at 02:37 UTC the criticality condition $\kappa_1 = 0.070$ was again satisfied (Fig.13) upon the occurrence of the ML(ATH)=3.2 EQ at 38.35^{o}N 21.94^{o}E. Approximately an hour later a ML(ATH)=5.0 or Ms(ATH)=5.5 (cf. USGS reported Mww=5.5) EQ occurred at 03:36 UTC, i.e., almost 44 days after the SES activity recorded at PAT on 4 January 2021. This is strikingly reminiscent of the evolution of the Killini-Vartholomio EQs in 1988, see Fig.28 of Ref.[9].

[92] *Note added on 21 October 2023.* On 13 October 2023 an additional SES activity was recorded at PIR depicted in Fig.14. In this figure, the relevant simultaneous raw data recordings at the central station of the telementric network for the PIR station at four channels are shown being surrounded by colored rectangles. Upon analyzing this signal in natural time, we find that it conforms to the aforementioned conditions (3) and (6) for its identification as an SES activity since the values $\kappa_1 = 0.069(3)$, $S = 0.066(3)$ ($< S_u$), and $S_- = 0.083(4)$ ($< S_u$) are deduced. The impending EQ should have an epicenter lying within the gray shaded area of Fig.1 showing the selectivity map of PIR measuring station and obeying the policy -concerning when a prediction is issued- summarized in Section 7.3 of Ref. [6], see also pages 155 and 171 of Ref.[28].

[93] *Note added on 16 November 2023.* In continuation of the previous Note, the following two EQs with magnitudes ML(ATH)=2.6 and 2.7 occurred today at 01:52 LT and 09:09 LT with epicenters at 34.57^{o}N 23.41^{o}E and 35.82^{o}N 22.22^{o}E, respectively, lying in the southern part of the PIR selectivity map (see Fig.6). The criticality condition $\kappa_1 = 0.070$ has been fulfilled today exhibiting magnitude threshold invariance for $M_{thres} = 2.2, 2.3, 2.4$ for the first EQ, when analyzing the seismicity within the PIR selectivity map after the SES activity on 13 October 2023, thus indicating that the critical point has been appoached.